



Mitigating Torsional Interactions with MMC Connected to Turbine-Generator Using a Novel Subsynchronous Damping Controller

K Shivashanker¹ M Janaki^{1*}

¹School of Electrical Engineering, Vellore Institute of Technology, Vellore, Tamil Nadu, India.

* Corresponding author's Email: janaki.m@vit.ac.in

Abstract: Modular multilevel converter (MMC) is a new potential power converter architecture for applications that require high voltage or high power. In investigating the subsynchronous resonance (SSR) characteristics of MMC, detailed small-signal modeling and control design is essential. This paper presents the detailed modeling of MMC in D - Q reference frame and analysis of SSR with MMC connected to a turbine-generator supplying a series compensated long AC transmission line. This paper proposes a novel subsynchronous damping controller (SSDC) that uses a band pass filter (BPF) to extract the subsynchronous frequency components of line current. These subsynchronous frequency components are then injected into the transmission line by an MMC controller, which suppresses them through the generator. Using D - Q model of the study system with a rating of 892.4 MVA at 60 Hz, eigenvalue analysis and transient simulation are used to perform SSR analysis for various series compensation levels from 0.20 p.u to 0.60 p.u in MATLAB-Simulink. The results of eigenvalue analysis are validated with transient simulation for a step disruption of 10% decrement in mechanical input of turbine-generator, which is employed at 0.50 sec and restored at 1.0 sec. Simulation results with MMC show that damping of torsional modes (TM_s) improves in high-frequency range of subsynchronous network mode (NM_{sub}), on the other hand, the damping of low-frequency TM_s reduces. Therefore, it is clear that the damping of torsional interactions increases with MMC. Finally, SSR characteristics are investigated with a novel SSDC connected to MMC that is activated at 1.50 sec. The results clearly demonstrate the improvement of critical TM_s in the system. Thereby reducing the potential risk of SSR at all operating conditions.

Keywords: Modular multilevel converter (MMC), Subsynchronous resonance (SSR), Small-signal modeling, Subsynchronous damping controller (SSDC).

1. Introduction

Series compensation is a widely used approach for improving the stability and thermal limitations of long AC transmission lines. Nevertheless, usage of series compensation may cause the subsynchronous resonance (SSR). SSR arises when frequency of an electrical mode of series compensated line matches with one of the torsional modes (TM_s) of a turbine-generator. The interaction between mechanical system and series compensated line can cause torsional oscillations on generator shafts, which can lead to fatigue and eventually failure if remain unattended [1, 2]. The HVDC interconnections are currently a well-remarkable alternative to long transmission AC line.

Voltage source converter based HVDC (VSC-HVDC) is increasing significantly in comparison to line commutated converter based HVDC (LCC-HVDC) due to its inherent benefits [3]. A VSC-HVDC connected to the turbine-generator doesn't cause potential risk of SSR when compared with conventional HVDC systems. In [4], analyzed the thorough investigation of SSR analysis caused by a VSC-HVDC connected close to turbine-generator units. Analysis of SSR was performed with inverter and rectifier operation of converter near turbine-generator. The results show that DC voltage control provides a small positive damping on SSR. A series compensated long AC transmission line and VSC based HVDC system are both originating from same substation are presented in [5], and a subsynchronous

current injector (SSCI) is proposed to mitigate subsynchronous frequency current components that flow through generator. The proposed SSCI improves damping of a system in the range of TM frequencies [5]. To analyze the effect of VSC-HVDC system on TMs of adjacent connected thermal generation units in [6], a state-space model of the system and an eigenvalue analysis are used and also proposed an adaptive subsynchronous frequency damping controller (SSFDC) to damp the multiple torsional modes.

Due to challenges in control schemes and practical constraints in VSC based HVDC systems, modular multilevel converters (MMCs) are implemented in HVDC transmission systems to meet wide-range power applications [7]. Compared with VSC, MMC have distinctive features like redundancy in operation, modularity, less switching losses, voltage level scalability, a significantly reduced THD, and improved response in output voltage [8, 9]. The modularity in design and other distinctive features enable MMC suitable for MMC based HVDC transmission systems, energy storage systems and FACTS devices [9]. When the MMCs are integrated into grids, harmonic resonance and instability can arise [10] due to the substantial second harmonics in control signals, capacitor voltages, arm currents of MMC and AC transmission line configurations. The resonance and instability can occur at different frequency levels (from a few Hz to kHz) depending on control dynamics [11]. Subsynchronous oscillation (SSO) is analyzed in wind farm that is integrated with an MMC based HVDC transmission system, and a stabilization control for mitigating SSO is proposed [12]. Proposed stabilization control technique suppresses SSO in wind farms connected to MMC-HVDC. The eigenvalue analysis is employed to study small-signal stability of MMC using state space models in [13–15]. In reference [16], a multiple phase margin contour plot method is proposed to investigate small-signal SSR for a DFIG-based wind power conversion system (WPCS) connected to MMC-HVDC system with various wind speeds. The results shows that damping of SSR decreases with decreasing wind speed. Reference [17] proposes a modal signal injection test to investigate subsynchronous torsional interactions (SSTI) between full-scale model of practical multi-terminal MMC-HVDC system and adjacent turbine-generator under different converter control schemes, loading levels, and coupling strength between AC networks & MMC-HVDC system. The results of full-scale model of MMC show that improved damping of

torsional modes when compared with the simplified models. A sub-synchronous oscillation damping controller is proposed in MMC-MTDC system for SSO suppression [18]. The results show SSDC increases electrical damping and thereby reduces potential risk of SSO at all critical modes. In [19], objective is to mitigate SSO in MMC-HVDC systems that integrate renewable energy by the use of MMC-based technology. To improve system stability and resilience, an extra sub-synchronous damping controller (ASSDC) based on Active Disturbance Rejection Control (ADRC) is proposed. The findings demonstrate that proposed ASSDC enhances the system's capacity to stabilize at a steady-state operating point more rapidly than systems without ASSDC. In [20], an MPC-based supplemental SSDC is proposed to study characteristics of SSO in MMC-HVDC linked to wind farms. The method successfully reduces SSOs, even when many oscillations occur at different frequencies. A state feedback decoupling control approach is proposed to mitigate SSO in wind farm integration with an MMC-HVDC transmission system [21]. The demonstrated control approach effectively decreases oscillations, thereby improving stability and the MMC-HVDC system's performance as well. The advanced digital power system simulator is used to develop a renewable energy base that is connected to a frail AC grid through an MMC-HVDC system [22]. The system's unstable oscillation risks are assessed using the Bode diagram and Nyquist diagram. In conclusion, it was inferred that SSO was observed between the renewable energy base and the MMC HVDC system. From references [12-22], it is noticed that subsynchronous oscillations/SSI or SSR characteristics are investigated in MMC-HVDC systems integrated with wind farms or other RES sources and MMC-MTDC system connected to grid.

This paper explores detailed modeling and investigation of SSR characteristics with MMC-HVDC connected to a multi-mass (six-mass) turbine-generator supplying a series compensated long AC transmission line. In modeling of an MMC-HVDC system, dynamics of MMC connected at PCC is modeled to investigate SSR characteristics, whereas far-end MMC dynamics of MMC-HVDC are neglected [12, 23, 24]. Accordingly, dynamics of MMC which is at far-end through DC link is represented as constant voltage source on DC side. The aim of our work is to investigate SSR characteristics of MMC connected turbine generator supplying a series compensated long AC transmission line for various series compensation

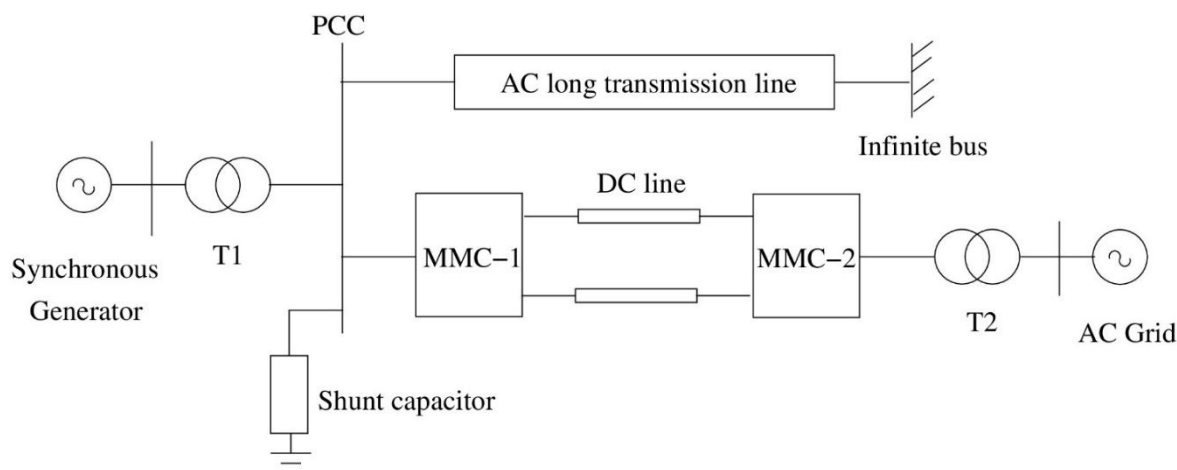


Figure. 1 Modified IEEE FBM with MMC based HVDC system and long AC transmission line originating from the same substation

levels. In this regard, detailed small-signal modeling and control design are essential. In $D-Q$ modeling of study system, the switching functions of MMC are estimated by fundamental and double fundamental frequency components, ignoring higher order harmonics. A method of control scheme is used to control the active and reactive power independently in AC system, and suppress the circulating currents in MMC phase-leg arms as well. Which is achieved through a cascaded control loops with cross-coupled current control loops in order to regulate fundamental and double fundamental frequency components of MMC output voltage. Later a novel SSDC is proposed to suppress subsynchronous frequency components pass through turbine generator. In this work, effectiveness of a controller for MMC, SSR characteristics with MMC, and a novel SSDC connected to MMC are analyzed with $D-Q$ model of study system using MATLAB-Simulink. SSR analysis is conducted for various series compensations from 0.20 p.u to 0.60 p.u with eigenvalue analysis and transient simulation. The results of eigenvalue analysis are validated with transient simulation for a step disruption of 10% decrement in mechanical input of turbine generator, which is employed at 0.50 sec and restored at 1.0 sec. The SSR characteristics with MMC show that damping of torsional modes (TMs) improves in high-frequency range of subsynchronous network mode (NM_{sub}), on the other hand, the damping of low-frequency TMs reduces. Therefore, it is clear that damping of torsional interactions increases with MMC. Finally, SSR characteristics are investigated with a novel SSDC connected to MMC that is activated at 1.50 sec. The results clearly demonstrate the improvement of critical TMs in the system. Thereby reducing the potential risk of SSR at all operating conditions.

The rest of paper presented as, study system and methods of SSR analysis are explained in Section 2, Section 3 describes the MMC modeling in $D-Q$ reference frame and controller for MMC, Section 4 illustrates analysis of SSR with MMC connected to multi-mass turbine-generator, the design of a novel SSDC using BPF is illustrated in Section 5, analysis of SSR with proposed SSDC connected to MMC is given in Section 6, Section 7 provides the conclusions.

2. Study system and methods of SSR analysis

The analysis of SSR characteristics with MMC connected to multi-mass turbine-generator supplying a series compensated transmission line requires a detailed modeling of the mechanical system and electrical system. The study system in this paper is modified from the IEEE First Benchmark Model (FBM) with MMC. Fig. 1 illustrates the simplification of the AC and DC dynamics of MMC-HVDC with an adjacent turbine generator to study the SSR characteristics. The dynamics of far-end converter of MMC-HVDC are neglected and represented as a constant voltage source as shown in Fig. 2(a). Fig. 2 is the simplified system to investigate the SSR with MMC nearby turbine-generator supplying a series compensated AC long transmission line. Study system (see Fig. 2(a)) comprises a multi-mass (six-mass) turbine-generator model (2.2), series compensated long AC transmission line, and MMC. Fig. 2(b) depicts a mechanical system (six-mass) of turbine-generator. The modeling of a detailed generator model (2.2) and six-mass mechanical system is explained in detail [2, 15] as illustrated in Fig. 2. The parameters of a study

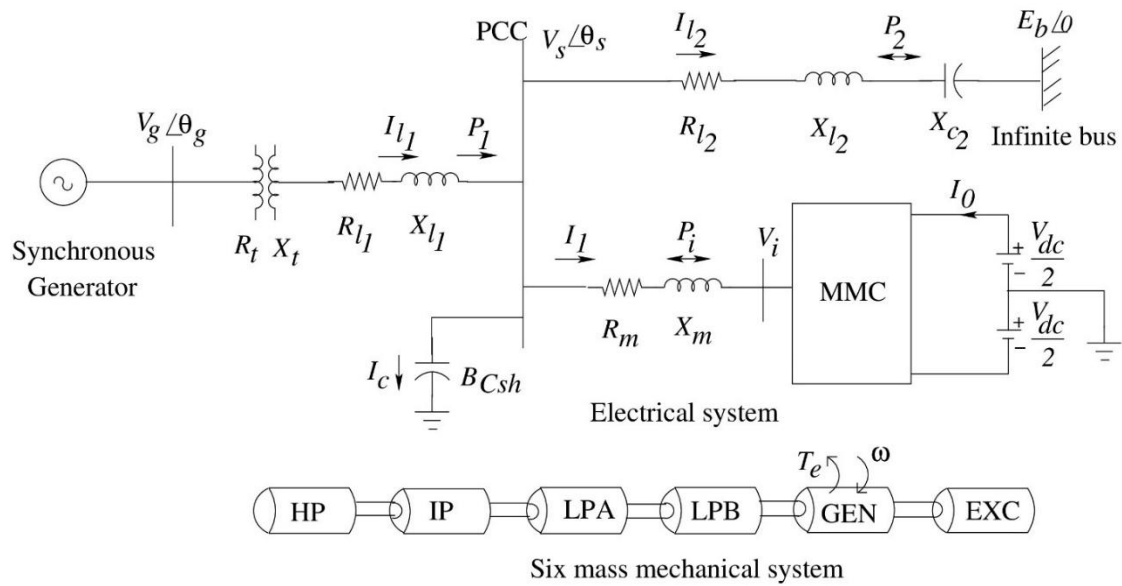


Figure. 2 Schematic diagram of the study system: (a) Electrical system and (b) Six mass mechanical system

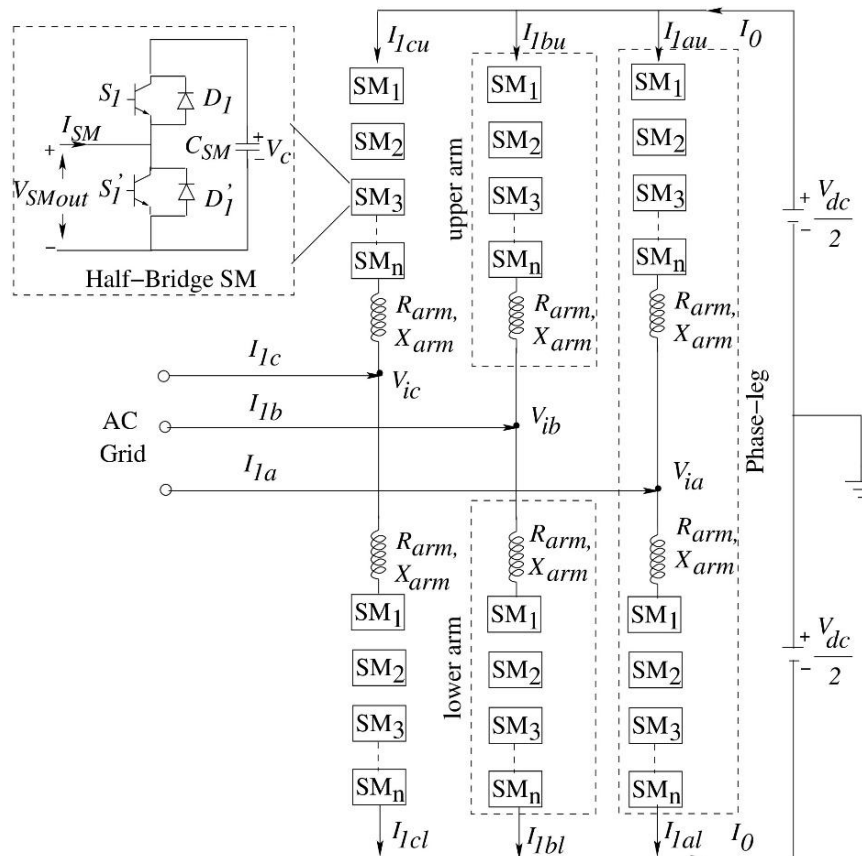


Figure. 3 Schematic representation of 3-Φ MMC

system is computed using the generator’s rated output of 892.4 MVA at 60 Hz [25].

The SSR analysis is carried out for different series compensation levels based on eigenvalue analysis and transient simulation analysis. Linearized models with eigenvalue analysis are used to

investigate steady-state SSR at the operating point. A thorough generator model (2.2) is used to account for the generator stator transients and also modeled transmission line using lumped inductance and resistance, with line transients taken into account to analyze the transient SSR. The study system equations at operating point are linearized, and

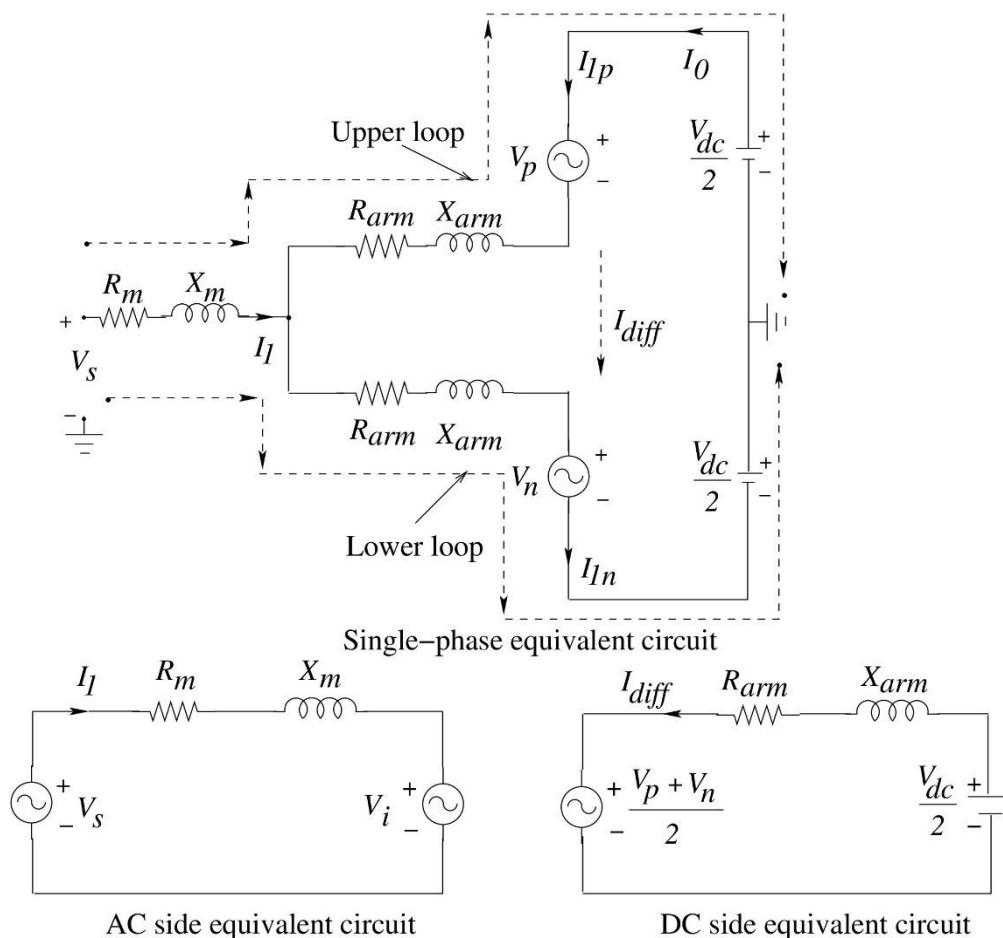


Figure. 4 Equivalent circuit of MMC: (a) 1- Φ equivalent circuit, (b) AC side equivalent circuit, and (c) DC side equivalent circuit

eigenvalues of a state matrix are computed. The location of system matrix's eigenvalues determines stability of a system. If all of the eigenvalues' real parts are negative, system is stable. The results of eigenvalue analysis are verified with a transient simulation of study system. The transient simulation analysis is evaluated using $D-Q$ model of the study system. The transient stability is evaluated by employing a disruption of 10% reduction in mechanical input to the multi-mass turbine-generator. The decreasing oscillatory time response shows transient stability of study system.

3. Modeling of MMC

The MMC typical diagram is illustrated in Fig. 3 [26-28]. MMC comprises three phase-legs. Two arms (lower and upper), each consists of a single series inductor and an 'n'-number of half-bridge submodules (HBSMs) that are coupled in a cascading fashion, form a phase-leg. A series inductor (arm inductor, X_{arm}) is used to limit circulating currents between arms (lower and upper) of each phase-leg.

As illustrated in Fig. 3, HBSM is an MMC building block composed of two switches (IGBTs) coupled in cascaded and one shunt capacitor. IGBTs function in a complimentary manner, according to their gate pulses. Fig. 4(a), (b), and (c) illustrates the single-phase equivalent circuit of MMC and its AC & DC equivalent circuits respectively [28]. The following subsections explain MMC modeling in the $D-Q$ reference frame, followed by MMC controllers.

3.1 Mathematical modeling of MMC in $D-Q$ reference frame

MMC is adequately modeled in a $D-Q$ reference frame to perform eigenvalue analysis. In $D-Q$ modeling, MMC switching functions are approximated by fundamental and double fundamental frequency components neglecting higher order harmonics.

Applying KVL to upper and lower loops in Fig. 4(a), the following two equations are obtained.

$$V_s - R_m I_1 - \frac{X_m}{\omega_B} \frac{dI_1}{dt} - R_{arm} I_{1p} + \frac{X_{arm}}{\omega_B} \frac{dI_{1p}}{dt} + V_p - \frac{V_{dc}}{2} = 0 \quad (1)$$

$$V_s - R_m I_1 - \frac{X_m}{\omega_B} \frac{dI_1}{dt} - R_{arm} I_{1n} + \frac{X_{arm}}{\omega_B} \frac{dI_{1n}}{dt} - V_n + \frac{V_{dc}}{2} = 0 \quad (2)$$

Fig. 4(a) is simplified into Fig. 4(b) and Fig. (c) as an AC and DC equivalent circuits of MMC. From which following equations are derived.

$$\frac{X_m}{\omega_B} \frac{dI_1}{dt} = V_s - (R_m + jX_m)I_1 - V_i \quad (3)$$

$$\frac{X_{arm}}{\omega_B} \frac{dI_{diff}}{dt} = \frac{V_{dc}}{2} - \frac{V_p + V_n}{2} - (R_{arm} + j2X_{arm})I_{diff} \quad (4)$$

Where

$$I_{diff} = I_0 + I_2 \quad (5)$$

Substituting Eq. (5) into Eq. (4), the following expression is derived.

$$\frac{X_{arm}}{\omega_B} \frac{d(I_0 + I_2)}{dt} = \frac{V_{dc}}{2} - \frac{V_p + V_n}{2} - (R_{arm} + j2X_{arm})(I_0 + I_2) \quad (6)$$

From Eqs. (3) and (6), the fundamental frequency current components, double fundamental frequency current components, and dc side current dynamics of MMC as given below are derived by separating different frequency components and transforming into the $D-Q$ reference frame using Kron's transformation [2].

$$\frac{X_m}{\omega_B} \frac{dI_{1D}}{dt} = V_{sD} - R_m I_{1D} - X_m I_{1Q} - V_{iD} \quad (7)$$

$$\frac{X_m}{\omega_B} \frac{dI_{1Q}}{dt} = V_{sQ} - R_m I_{1Q} + X_m I_{1D} - V_{iQ} \quad (8)$$

$$\frac{X_{arm}}{\omega_B} \frac{dI_{2D}}{dt} = -R_{arm} I_{2D} - 2X_{arm} I_{2Q} - V_{cirD} \quad (9)$$

$$\frac{X_{arm}}{\omega_B} \frac{dI_{2Q}}{dt} = -R_{arm} I_{2Q} + 2X_{arm} I_{2D} - V_{cirQ} \quad (10)$$

$$\frac{X_{arm}}{\omega_B} \frac{dI_0}{dt} = \frac{V_{dc}}{2} - \frac{nV_{c0}}{2} + \frac{nV_{1Q}V_{c1Q}}{2V_{dc}} + \frac{nV_{1D}V_{c1D}}{2V_{dc}} - \frac{nV_{2Q}V_{c2Q}}{2V_{dc}} - \frac{nV_{2D}V_{c2D}}{2V_{dc}} - R_{arm} I_0 \quad (11)$$

Similarly, the dynamics of DC side namely dc, fundamental, and double fundamental frequency

components of SM capacitor voltages are derived in $D-Q$ reference frame as given below [13].

$$\frac{B_c}{\omega_B} \frac{dV_{c0}}{dt} = \frac{I_0}{2} + \frac{V_{1D}I_{1D}}{4V_{dc}} + \frac{V_{1Q}I_{1Q}}{4V_{dc}} + \frac{V_{2D}I_{2D}}{2V_{dc}} + \frac{V_{2Q}I_{2Q}}{2V_{dc}} \quad (12)$$

$$\frac{B_c}{\omega_B} \frac{dV_{c1D}}{dt} = -\frac{I_{1D}}{4} - \frac{V_{1D}I_0}{V_{dc}} + \frac{V_{2D}I_{1Q}}{4V_{dc}} + \frac{V_{2Q}I_{1D}}{4V_{dc}} + \frac{V_{1D}I_{2Q}}{2V_{dc}} + \frac{V_{1Q}I_{2D}}{2V_{dc}} + B_c V_{c1Q} \quad (13)$$

$$\frac{B_c}{\omega_B} \frac{dV_{c1Q}}{dt} = -\frac{I_{1Q}}{4} - \frac{V_{1Q}I_0}{V_{dc}} - \frac{V_{2Q}I_{1Q}}{4V_{dc}} + \frac{V_{2D}I_{1D}}{4V_{dc}} - \frac{V_{1Q}I_{2Q}}{2V_{dc}} + \frac{V_{1D}I_{2D}}{2V_{dc}} - B_c V_{c1D} \quad (14)$$

$$\frac{B_c}{\omega_B} \frac{dV_{c2D}}{dt} = \frac{I_{2D}}{2} + \frac{V_{2D}I_0}{V_{dc}} + \frac{V_{1D}I_{1Q}}{4V_{dc}} + \frac{V_{1Q}I_{1D}}{4V_{dc}} + 2B_c V_{c2Q} \quad (15)$$

$$\frac{B_c}{\omega_B} \frac{dV_{c2Q}}{dt} = \frac{I_{2Q}}{2} + \frac{V_{2Q}I_0}{V_{dc}} + \frac{V_{1Q}I_{1Q}}{4V_{dc}} - \frac{V_{1D}I_{1D}}{4V_{dc}} - 2B_c V_{c2D} \quad (16)$$

$D-Q$ components of MMC output voltage are expressed below as

$$V_{iD} = -\frac{nV_{c1D}}{2} + \frac{nV_{1D}V_{c0}}{V_{dc}} - \frac{nV_{1D}V_{c2Q}}{2V_{dc}} - \frac{nV_{1Q}V_{c2D}}{2V_{dc}} + \frac{nV_{2D}V_{c1Q}}{2V_{dc}} + \frac{nV_{2Q}V_{c1D}}{2V_{dc}} \quad (17)$$

$$V_{iQ} = -\frac{nV_{c1Q}}{2} + \frac{nV_{1Q}V_{c0}}{V_{dc}} + \frac{nV_{1Q}V_{c2Q}}{2V_{dc}} - \frac{nV_{1D}V_{c2D}}{2V_{dc}} - \frac{nV_{2Q}V_{c1Q}}{2V_{dc}} + \frac{nV_{2D}V_{c1D}}{2V_{dc}} \quad (18)$$

$D-Q$ components of MMC circulating voltage are expressed below as

$$V_{cirD} = \frac{nV_{c2D}}{2} - \frac{nV_{1D}V_{c1Q}}{2V_{dc}} - \frac{nV_{1Q}V_{c1D}}{2V_{dc}} + \frac{nV_{2D}V_{c0}}{V_{dc}} \quad (19)$$

$$V_{cirQ} = \frac{nV_{c2Q}}{2} - \frac{nV_{1Q}V_{c1Q}}{2V_{dc}} + \frac{nV_{1D}V_{c1D}}{2V_{dc}} + \frac{nV_{2Q}V_{c0}}{V_{dc}} \quad (20)$$

The $D-Q$ model of MMC is developed with equations from Eq. (7) to Eq. (20) in MATLAB-Simulink.

3.2 MMC controller

The controller for MMC [28] is designed to control fundamental frequency components of MMC output voltage, and to suppress circulating currents that pass-through phase-legs of MMC. Control structure for MMC is shown in Fig. 5. The following subsections give more insight about the structure of MMC controller.

3.2.1 Fundamental frequency current components control

A scheme of MMC control is used to control active and reactive powers independently. Proposed power decoupled control consists of a cascaded control loops with cross-coupled current control loops. The controller for fundamental frequency current components is designed based on equations, Eq. (7) and Eq. (8). The control structure of MMC fundamental frequency current component is explored in Fig. 5. Referring to Fig. 5, reference values of quadrature and direct axes currents (I_{IQRef} and I_{IDRef}) are obtained from active and reactive power (P_i and Q_i) controllers. The P_i and Q_i contributed by fundamental frequency component are calculated using equations, Eq. (21) and Eq. (22) as given below

$$P_i = V_{iD}I_{iD} + V_{iQ}I_{iQ} \tag{21}$$

$$Q_i = V_{iD}I_{iQ} - V_{iQ}I_{iD} \tag{22}$$

The reference value of MMC output voltage at fundamental frequency are expressed in $D-Q$ reference frame given below as

$$V_{1Dref} = \frac{1}{(nV_{c0} - \frac{n}{2}V_{c2Q})} \left[V_{iD}V_{dc} + \frac{n}{2}(V_{c1D}V_{dc} - V_{2D}V_{c1Q} - V_{2Q}V_{c1D} + V_{1Q}V_{c2D}) \right] \tag{23}$$

$$V_{1Qref} = \frac{1}{(nV_{c0} + \frac{n}{2}V_{c2Q})} \left[V_{iQ}V_{dc} + \frac{n}{2}(V_{c1Q}V_{dc} - V_{2D}V_{c1D} + V_{2Q}V_{c1Q} + V_{1D}V_{c2D}) \right] \tag{24}$$

3.2.2 Circulating current control

Circulating current controller for MMC is explored in Fig. 5. The circulating current controller is designed based on equations, Eq. (9) and Eq. (10) to reduce the second harmonic currents in arm currents of MMC. The active and reactive power contributed by double fundamental frequency components are given below as

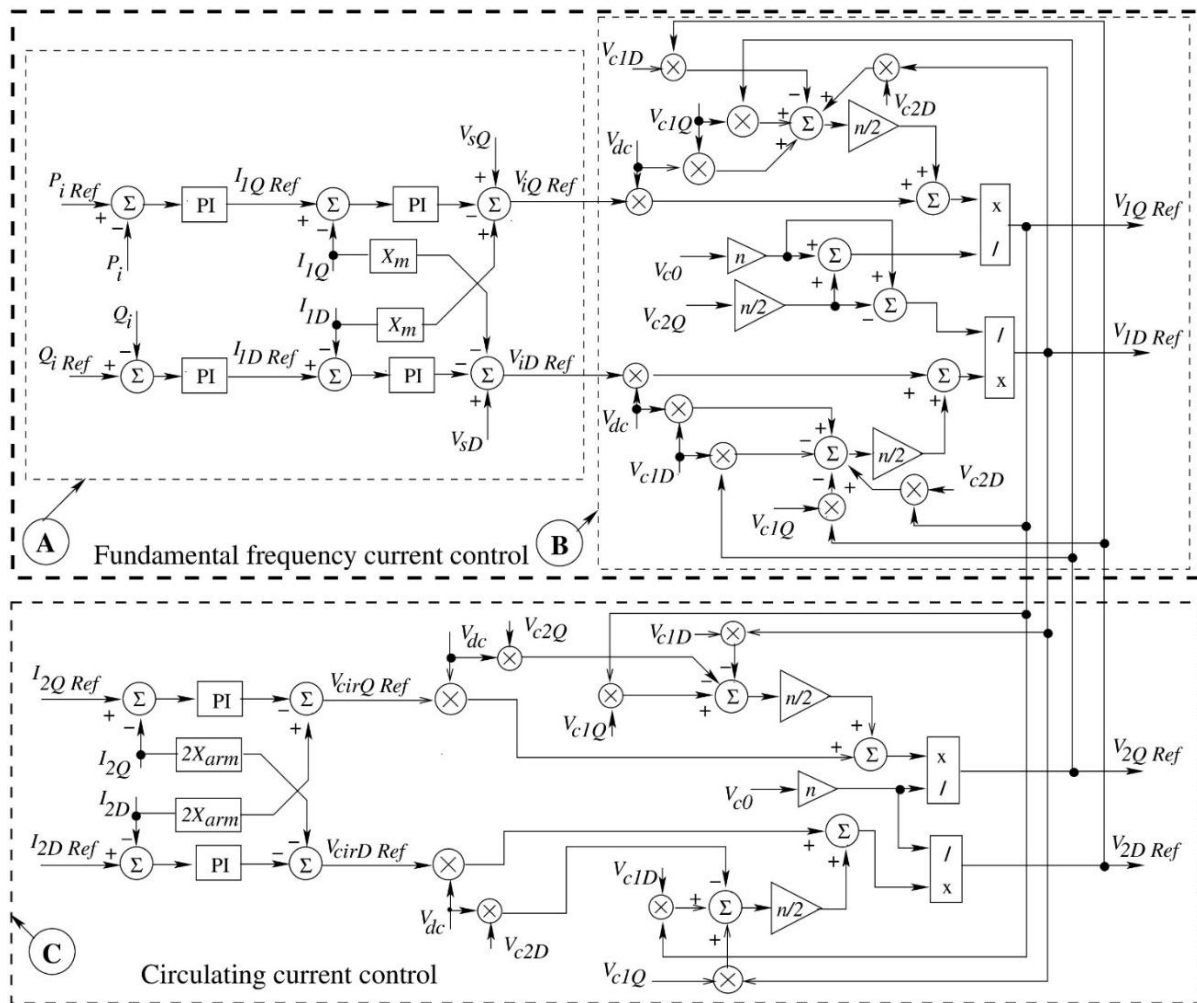


Figure. 5 Controller for MMC

$$P_2 = V_{cirD}I_{2D} + V_{cirQ}I_{2Q} \tag{25}$$

$$Q_2 = V_{cirD}I_{2Q} - V_{cirQ}I_{2D} \tag{26}$$

The reference value of MMC voltage components corresponding to double fundamental frequency is expressed in $D-Q$ reference frame given below as

$$V_{2Dref} = \frac{1}{nV_{co}} \left[V_{cirD}V_{dc} + \frac{n}{2} (-V_{c2D}V_{dc} + V_{1D}V_{c1Q} + V_{1Q}V_{c1D}) \right] \tag{27}$$

$$V_{2Qref} = \frac{1}{nV_{co}} \left[V_{cirQ}V_{dc} + \frac{n}{2} (-V_{c2Q}V_{dc} - V_{1D}V_{c1D} + V_{1Q}V_{c1Q}) \right] \tag{28}$$

4. Analysis of SSR

SSR characteristics of MMC with series compensated transmission line is investigated with $D-Q$ model of study system using eigenvalue analysis and transient simulation. Relying on linearized model, eigenvalue analysis is evaluated to examine small-signal stability of study system at an equilibrium point. The eigenvalue analysis is examined without and with MMC for different series compensation levels. The results of eigenvalue analysis are validated with transient simulation. Which is performed for a step disruption of 10% decrement in the mechanical input of turbine-generator. The following subsections explains the eigenvalue analysis and transient simulation in detail.

4.1 Eigenvalue analysis

The state matrix of a linearized study system is used to determine its eigenvalues. The location of the state matrix's eigenvalues determines small-signal stability. System is stable if all real part of eigenvalue is negative. To evaluate maximum undamping of TMs, eigenvalue analysis is examined with series compensation (X_{c2}) from 0.20 p.u to 0.60 p.u. Fig. 6 shows movement of TMs and subsynchronous network mode (NM_{sub}) eigenvalues real parts with the variation in X_{c2} with MMC. Referring to Fig. 6, it is evident that torsional modes ($TM-1$ to $TM-4$) are unstable for a certain range of series compensation. From Fig. 6, the series compensation levels corresponding to maximum undamping of torsional modes are noted to perform eigenvalue analysis and transient simulation to investigate adverse torsional interactions. Results of eigenvalue analysis with distinct series compensation levels for without and with MMC are shown in Tables 1. Referring to the Table 1, it is noticed that, with $X_{c2} = 0.29$ p.u

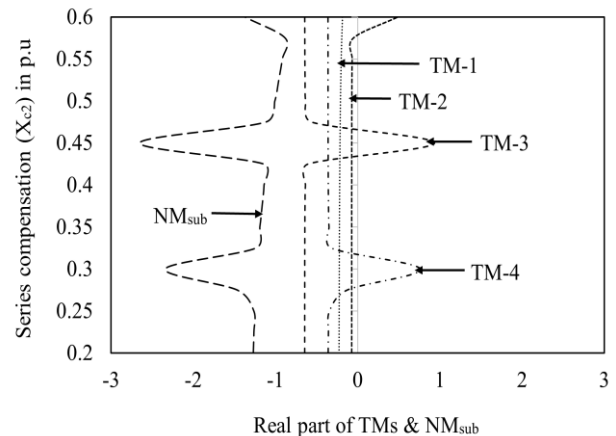


Figure. 6 Movement of the TMs and NM_{sub} eigenvalues real parts with the variation in series compensation

Table 1. Eigenvalues of the study system without and with MMC for different series compensations

Torsional Mode	Without MMC		With MMC	
	$X_{c2}=0.29$ p. u	$X_{c2}=0.45$ p. u	$X_{c2}=0.29$ p. u	$X_{c2}=0.45$ p. u
0	$-1.67860 \pm j 7.6252$	$-2.01640 \pm j 8.2122$	$-1.27980 \pm j 7.1313$	$-1.54490 \pm j 7.8058$
1	$-0.22961 \pm j 99.051$	$-0.22355 \pm j 99.163$	$-0.22468 \pm j 99.016$	$-0.21513 \pm j 99.136$
2	$-0.07415 \pm j 127.02$	$-0.07431 \pm j 127.04$	$-0.07378 \pm j 127.02$	$-0.07338 \pm j 127.04$
3	$-0.64447 \pm j 160.62$	$1.14380 \pm j 161.18$	$-0.64447 \pm j 160.62$	$0.93040 \pm j 160.88$
4	$1.28670 \pm j 203.19$	$-0.36266 \pm j 202.83$	$1.18150 \pm j 203.05$	$-0.36025 \pm j 202.80$
5	$-1.85040 \pm j 298.17$			
NM_{sub}	$-2.45720 \pm j 203.26$	$-2.20810 \pm j 161.11$	$-2.77010 \pm j 203.12$	$-2.65520 \pm j 160.96$
NM_{super}	$-1.57070 \pm j 550.31$	$-1.60070 \pm j 592.23$	$-1.99400 \pm j 550.16$	$-2.26680 \pm j 592.01$

frequency of NM_{sub} is close to $TM-4$. Thus $TM-4$ is unstable. With $X_{c2}=0.45$ p.u, it is observed that NM_{sub} frequency is close to $TM-3$. Therefore $TM-3$ is unstable. In Table 1, it is noticed that the frequency of NM_{sub} slightly reduces with MMC, while the damping improves. However, damping of TMs in low frequency range of NM_{sub} reduces, while improves in high frequency range. As the lower frequency TMs are more critical, the torsional interactions are expected to be more severe with inclusion of MMC.

4.2 Transient simulation

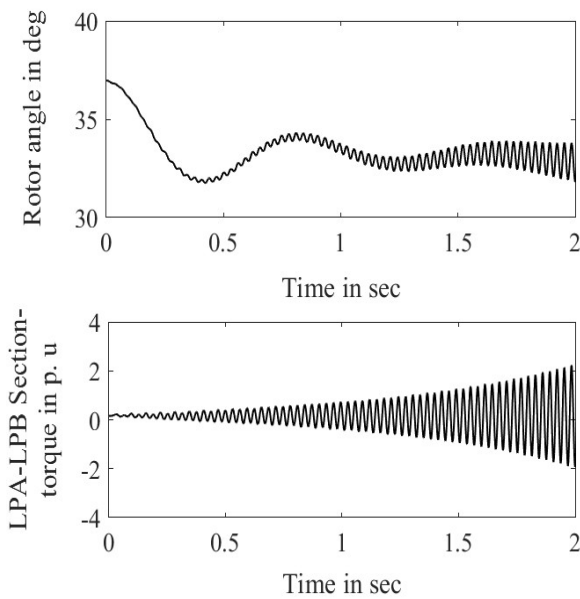


Figure. 7 Response of rotor angle and shaft section (LPA-LPB) torque for step disruption in mechanical input with $X_{c2} = 0.29$ p.u for without MMC

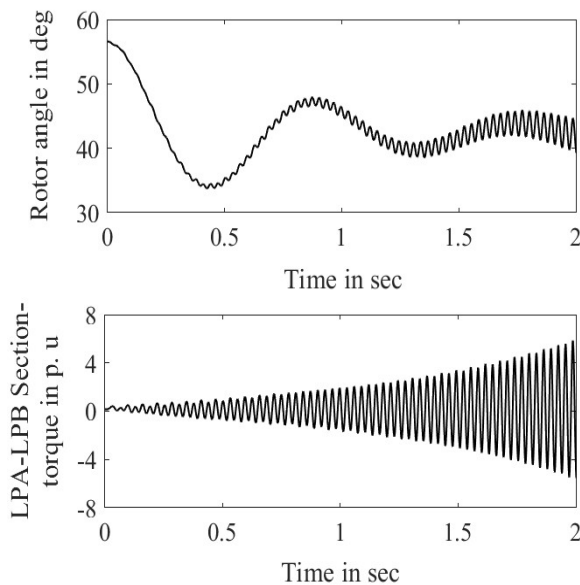


Figure. 8 Response of rotor angle and shaft section (LPA-LPB) torque for step disruption in mechanical input with $X_{c2} = 0.29$ p.u for with MMC

Transient simulation is used to verify the results of eigenvalue analysis. A step disruption of 10% reduction in mechanical input of a multi-mass turbine-generator employed at 0.50 sec and reverted at 1.0 sec for without and with MMC. Simulation results of rotor angle and section torque (LPA-LPB) for the step disruption in mechanical input with series compensation (X_{c2}) of 0.29 p.u are shown in Fig. 7 and Fig. 8 for without and with MMC. Referring to Figs. 7 and 8, it is to be noticed that magnitude of oscillations in section torque (LPA-LPB) is higher

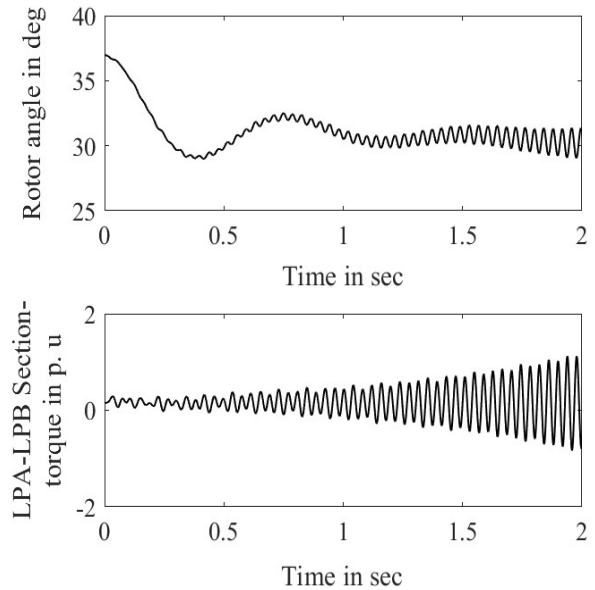


Figure. 9 Response of rotor angle and shaft section (LPA-LPB) torque for step disruption in mechanical input with $X_{c2} = 0.45$ p.u for without MMC

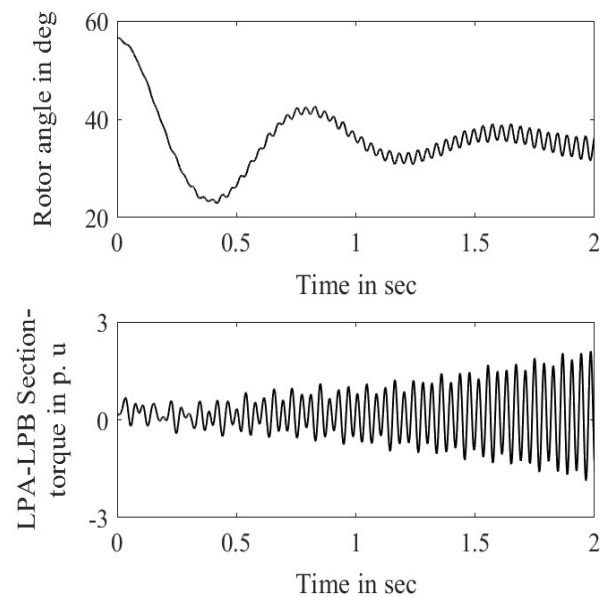


Figure. 10 Response of rotor angle and shaft section (LPA-LPB) torque for step disruption in mechanical input with $X_{c2} = 0.45$ p.u for with MMC

with MMC. Figs. 9 and 10 shows the response of rotor angle and section torque (LPA-LPB) for the step disruption in mechanical input with $X_{c2} = 0.45$ p.u for without and with MMC. Referring to Figs. 9 and 10, it is to be noticed that the oscillatory response of section torque (LPA-LPB) is growing faster with MMC. Thus, it is evident that damping of torsional interactions grows faster with MMC.

5. Design of a novel Subsynchronous Damping Controller (SSDC)

This paper proposed a novel subsynchronous damping controller (SSDC) that uses a band pass filter (BPF) to mitigate subsynchronous interactions in the range of TM frequencies. Block diagram of a novel BPF based SSDC is shown in Fig. 11. The proposed SSDC consists of one pair of BPFs for each TM in $D-Q$. It is also to be noted that, the power converters interact with series compensated transmission line as well as the torsional system of turbine-generator. Hence, it is required to improve the damping of TMs and subsynchronous network mode (NM_{sub}) as well. Accordingly, novel SSDC is

designed with separate BPFs for each TM and a common BPF for both NM_{sub} and TMs in the range of critical TM frequencies. In this work, IEEE FBM with inclusion of MMC is adapted, which have five natural TM frequencies [2]. Pass band of the filter is determined by eigenvalue analysis with the TM frequency is taken into account as center frequency. Bandwidth of TM filters is chosen in the range of 2 to 5 Hz, whereas the bandwidth of common filters is chosen to be the range of TM frequencies in order to enhance damping of all TMs and NM_{sub} in the practical range of series compensation.

Gains of the proposed SSDC are selected through eigenvalue analysis based on the criteria that all the eigenvalues should be stable in the practical spectrum (0-75%) of series compensation. Common filters enable the coarse adjustment of gains over the range of TM frequencies, whereas filters of individual TM enable fine adjustment of gain which is effective on the corresponding TM . The damping of critical TMs is increased by extracting subsynchronous frequency current components of transmission line and injected into transmission network that pass through an MMC

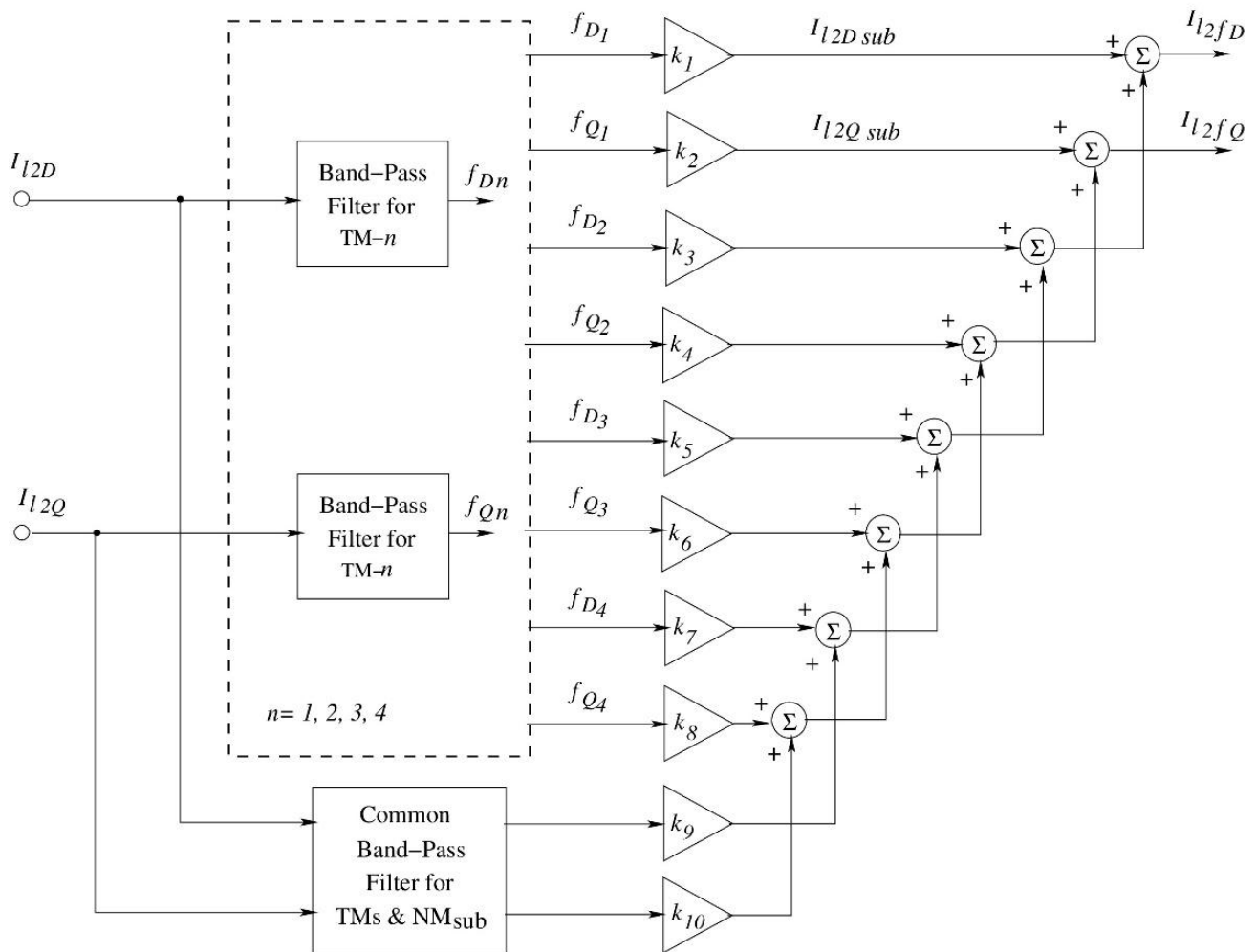


Figure. 11 Structure of a novel BPF based SSDC

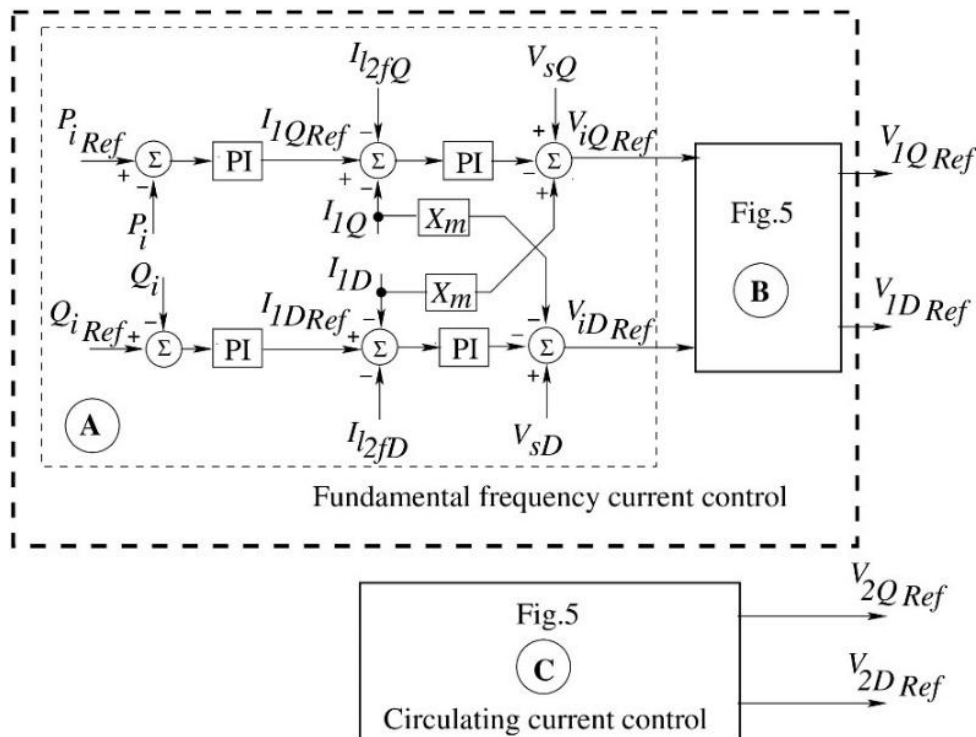


Figure. 12 Controller for MMC with extracted subsynchronous frequency components from SSDC

controller. Thereby suppresses subsynchronous frequency currents that go through a generator. It is worth noting that the TM becomes unstable for NM_{sub} frequencies that are closer to the critical TM frequency. Proposed SSDC uses five BPFs to extract the I_{12Dsub} and I_{12Qsub} of each torsional frequency component from line currents I_{12D} and I_{12Q} . Each filter set enhances damping of its associated TM by decreasing negative damping and is only effective for the frequency of its corresponding TM .

The novel SSDC extracts subsynchronous frequency current components that correspond to TMs 1, 2, 3, and 4 passes them through suitable gains (K_1 to K_{10}) to obtain I_{12fD} and I_{12fQ} . The signal is then summed to obtain I_{12fD} and I_{12fQ} , as given below:

$$I_{12fD} = \sum_m I_{12Dsub} \tag{29}$$

$$I_{12fQ} = \sum_m I_{12Qsub} \tag{30}$$

where $m = 1, 2, 3,$ and 4 (TMs).

Since $TM-5$ has a very high modal inertia, $TM-5$ is never excited, thus it is not desirable to extract the $TM-5$ frequency component using a filter. The extracted subsynchronous currents (I_{12fD} and I_{12fQ}) are injected into the line through MMC controller as depicted in Fig. 12. Following section presents SSR analysis with proposed SSDC connected to MMC.

6. Analysis of SSR with a novel subsynchronous damping controller

SSR characteristics with a novel SSDC connected to MMC linked nearby turbine generator supplying a series compensation line are investigated in this section. SSR characteristics are examined using eigenvalue analysis and transient simulation for various series compensation levels from 0.20 p.u to 0.60 p.u. in MATLAB-Simulink. Eigenvalue analysis outcomes are validated using transient simulation for a step disruption of 10% decrement in the mechanical input of turbine-generator. Following subsections give more insights on eigenvalue analysis and transient simulation with a novel SSDC connected to MMC.

6.1 Eigenvalue analysis

Eigenvalue analysis is performed with a novel SSDC connected to MMC using study system's linearized model. The results of the eigenvalue analysis for different series compensation levels with proposed SSDC connected to MMC linked nearby turbine generator supplying a series compensation line are illustrated in Table 2.

Referring to Table 2, it is evident that for lower and higher series compensation levels, all real parts of eigenvalues are negative. Therefore, study system is stable with a novel SSDC connected to MMC.

Table 2. Eigenvalues of study system with proposed SSDC connected to MMC for different series compensations

TM	With a novel SSDC connected to MMC	
	$X_{c2}=0.29$ p. u	$X_{c2}=0.45$ p. u
0	$-1.2819 \pm j 7.1647$	$-1.5520 \pm j 7.8417$
1	$-0.2331 \pm j 99.014$	$-0.2607 \pm j 99.144$
2	$-0.0725 \pm j 127.02$	$-0.0723 \pm j 127.04$
3	$-0.6073 \pm j 160.62$	$-0.4569 \pm j 160.43$
4	$-0.2287 \pm j 202.77$	$-0.3506 \pm j 202.79$
5	$-1.8504 \pm j 298.17$	$-1.8504 \pm j 298.17$
NM_{sub}	$-3.0650 \pm j 194.28$	$-1.3668 \pm j 150.76$
NM_{super}	$-0.7764 \pm j 545.88$	$-1.1082 \pm j 587.06$

Comparing the eigenvalue analysis results of Table 1 (without SSDC) with Table 2 (with a novel SSDC connected to MMC), the observations are made as follows:

- The damping of $TM-4$ and $TM-3$ are significantly improved with a novel SSDC connected to MMC for $X_{c2} = 0.29$ p.u. and $X_{c2} = 0.45$ p.u. as well.
- The frequency of NM_{sub} reduces with a novel SSDC connected to MMC.
- $TM-5$ is not excited since Mode-5 has very high modal inertia.
- With a novel SSDC connected to MMC, eigenvalues of all TM_s have the negative real parts for different series compensation levels. Hence the system is stable.

6.2 Transient simulation

The outcomes of eigenvalue analysis are validated using transient simulation with a novel SSDC connected to an MMC-linked nearby turbine generator supplying a series compensation line in MATLAB-Simulink. Transient simulation is carried out with a novel SSDC connected to MMC for a step disruption of 10% decrement in mechanical input of the multi-mass turbine-generator employed at 0.50 sec and restored at 1.0 sec. Simulation results of rotor angle and section torque (LPA-LPB) for step disruption in mechanical input with different series compensations are shown in Fig. 13 and Fig. 14 for the proposed SSDC connected to MMC is activated at 1.50 sec. Referring to Figs. 13 and 14, it is noticed that the responses of rotor angle and section torque (LPA-LPB) are growing oscillatory until the proposed SSDC is switched-on at 1.50 sec. After activation of the proposed SSDC at 1.50 sec,

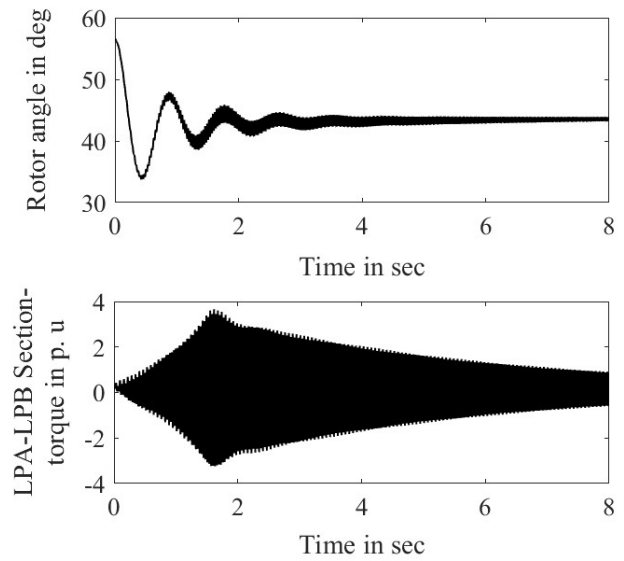


Figure. 13 Variation of rotor angle and section (LPA-LPB) torque and for step disruption in mechanical input for $X_{c2} = 0.29$ p.u with SSDC connected to MMC activated at 1.50 sec

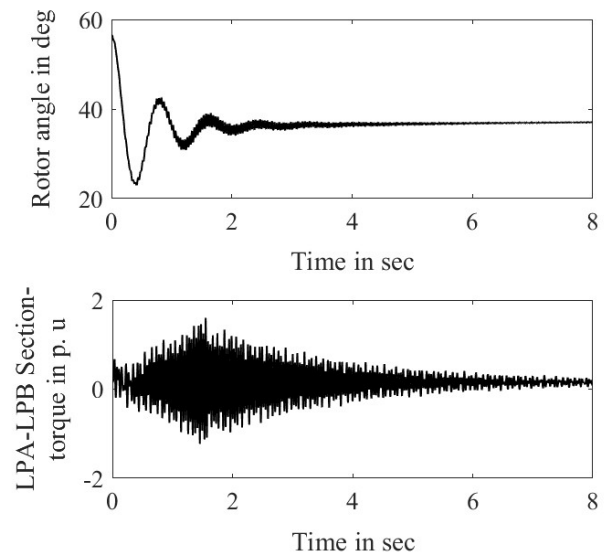


Figure. 14 Variation of rotor angle and section torque (LPA-LPB) for step disruption in mechanical input for $X_{c2} = 0.45$ p.u with SSDC connected to MMC activated at 1.50 sec

magnitude of oscillations of section torque (LPA-LPB) are reduced over time. Therefore, it is evident that proposed SSDC suppresses subsynchronous currents flowing from a transmission line to the generator. Thereby mitigating subsynchronous interactions. The results of transition simulation are consistent with those of the eigenvalue analysis.

To validate the transient simulation results, FFT analysis is carried out on LPA-LPB section torque. In this regard, data from transient simulation of section torque (LPA-LPB) with a novel SSDC connected to MMC is used. The FFT analysis is performed in the

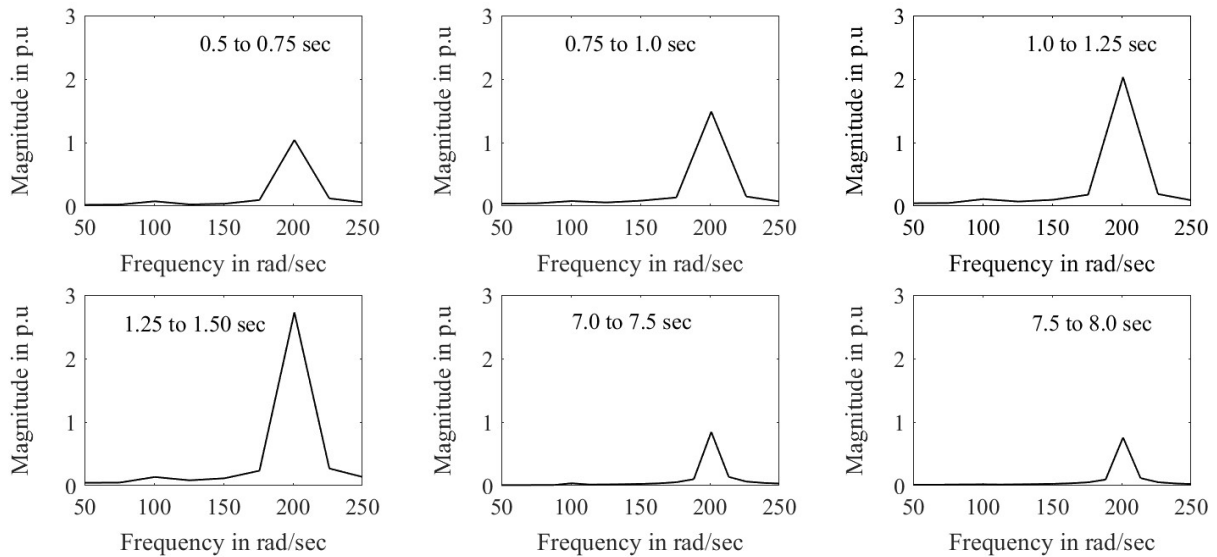


Figure. 15 FFT analysis of section torque (LPA-LPB) with $X_{c2} = 0.29$ p.u for SSDC connected to MMC activated at 1.50 sec

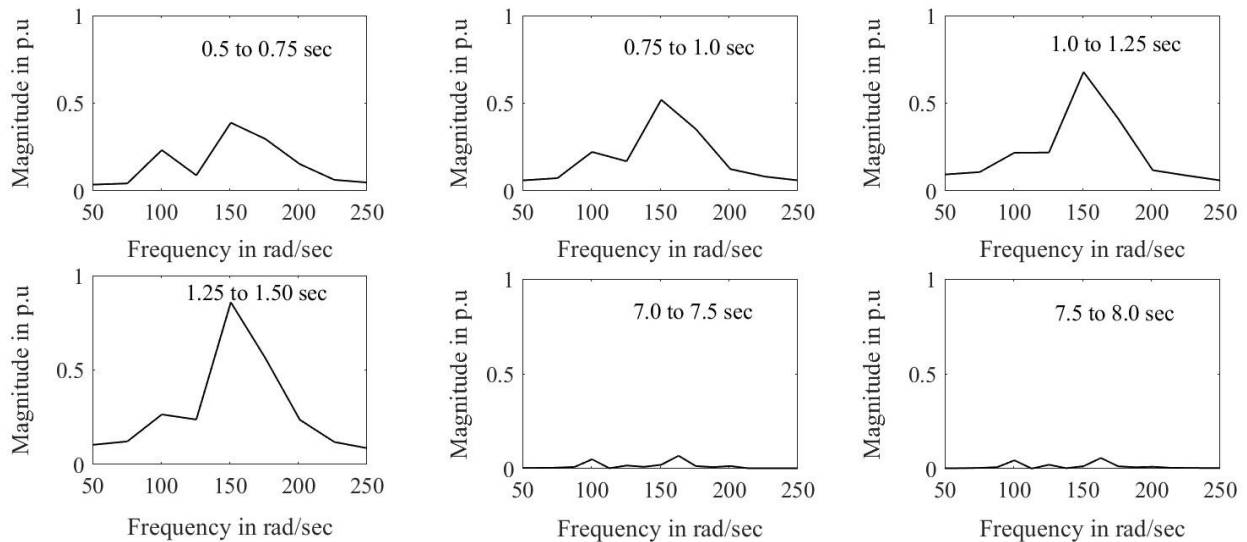


Figure. 16 FFT analysis of section torque (LPA-LPB) with $X_{c2} = 0.45$ p.u for SSDC connected to MMC activated at 1.50 sec

time interval of 0.50 to 8.0 sec with a time difference of 0.25 sec until the proposed SSDC activation at 1.50 sec, after that time interval of 0.50 sec is taken. The results of FFT analysis for different series compensation levels is shown in Fig. 15 and Fig. 16. Referring to Fig. 15 it is to be noted that, at $X_{c2} = 0.29$ p.u the magnitude in LPA-LPB section torque about 200 rad/sec is increasing with time. This frequency of oscillations corresponds to TM-4. When the proposed SSDC is switched-on at 1.50 sec, magnitude of section torque decreases with time. From Fig. 16 it is evident that Mode-3 component for $X_{c2} = 0.45$ p.u rises with time. When SSDC is triggered at 1.50 sec, Mode-3 component gradually decays over time. Based on FFT analysis, it is noticed that a novel

SSDC's potent in suppressing subsynchronous frequency current components flowing from transmission line to the turbine generator.

7. Conclusion

This paper presents detailed modeling and investigation of SSR characteristics with MMC connected to a six-mass turbine-generator supplying a series compensated long AC transmission line. In detailed modeling, the study system is modeled in a $D-Q$ reference frame using MATLAB-Simulink. The controller for MMC is designed including SM capacitor dynamics to control the active and reactive power independently in AC system and suppress the

circulating currents that flow between arms of each MMC phase-legs as well. SSR characteristics are investigated with MMC connected to turbine generator supplying a series compensated AC long transmission line for various series compensations from 0.20 p.u to 0.60 p.u using eigenvalue analysis and transient simulation. Results of eigenvalue analysis are verified with transient simulation for a step disruption of 10% decrement in mechanical input of turbine generator employed at 0.50 sec and restored at 1.0 sec. Results show that the damping of torsional interactions grows faster with MMC. Finally, a novel SSDC using BPF is designed to extract subsynchronous frequency current components from a transmission line. SSR characteristics are carried out with a novel SSDC connected to MMC that is activated at 1.50 sec for different series compensation levels.

The following results are observed with small-signal modeling of MMC connected to turbine generator supplying a series compensated long AC transmission line using MATLAB-Simulink.

- The frequency of NM_{sub} slightly reduces with MMC, while the damping improves in comparison to without MMC.
- Damping of TMs in the low-frequency range of NM_{sub} reduces, while improves in high-frequency range in comparison to without MMC.
- The frequency of NM_{sub} reduces with a novel SSDC connected to MMC.
- The eigenvalues of all critical TMs are stable with a novel SSDC connected to MMC. Hence, study system is stable.
- Transient simulation with a novel SSDC suppresses the subsynchronous currents that are flowing from a transmission line to generator. Thereby mitigating subsynchronous interactions in the study system.
- Transient simulation results show satisfactory responses with a novel BPF-based SSDC and are consistent with the eigenvalue analysis results.

Conflicts of Interest

The authors declare no conflict of interest.

Author Contributions

Conceptualization, K Shivashanker and M Janaki; methodology, K Shivashanker; software, K Shivashanker; validation, M Janaki; formal analysis, K Shivashanker; investigation, M Janaki; resources,

M Janaki; data curation, K Shivashanker; writing-original draft preparation, K Shivashanker; writing-review and editing, M Janaki; visualization, K Shivashanker; supervision, M Janaki; project administration, M Janaki.

Nomenclature

$d, q \text{ \& } D, Q$	Subscripts to denote direct and quadrature components in machine and network reference frame
$ V_g , E_b $	Magnitude of generator terminal voltage, infinite bus voltage
$ V_s $	Magnitude of point of common coupling (PCC) voltage
$ V_i $	Magnitude of MMC output voltage
V_{gd}, V_{gq}	Generator terminal voltages
ω	Generator rotor speed
ω_B	Base angular frequency
T_e	Electrical torque
V_{sD}, V_{sQ}	PCC voltages
$\theta_g, \theta_b, \theta_s$	Phase angle of generator terminal voltage, infinite bus voltage, PCC voltage
V_{iD}, V_{iQ}	MMC output voltages
R_t, X_t	Resistance and inductive reactance of transformer
R_{l1}, X_{l1}	Resistance and inductive reactance of the line between a transformer and PCC
R_{l2}, X_{l2}	Resistance and inductive reactance of the line between infinite bus and PCC
I_{l1D}, I_{l1Q}	Line current flow between generator terminal and PCC
I_{l2D}, I_{l2Q}	Line current flow between PCC and infinite bus
I_c	Shunt capacitor current
I_{l2fD}, I_{l2fQ}	Synthesized subsynchronous frequency current components of line
I_{l2Dsub}, I_{l2Qsub}	Subsynchronous frequency current components of line
B_{Csh}	Susceptance of shunt capacitor
R_m, X_m	Resistance and inductive reactance of the line between MMC and PCC
R_{arm}, X_{arm}	Arm resistance and inductive reactance of MMC
I_{l1}, I_{l1p}	Lower and upper arm currents of MMC
$I_{1D}, I_{1Q} \text{ \& } I_{2D}, I_{2Q}$	Fundamental and double fundamental frequency current components of MMC

I_{diff}	Inner unbalanced current of MMC phase-leg
I_0	DC side current
V_{cirD}, V_{cirQ}	MMC circulating voltages
V_{dc}	DC side voltage
V_{1D}, V_{1Q}	Fundamental frequency components of controlled output voltages of MMC
V_{2D}, V_{2Q}	Double fundamental frequency components of controlled output voltages of MMC
V_{c0}	DC component of SM capacitor voltage
V_{c1D}, V_{c1Q}	Fundamental frequency components of SM capacitor voltages
V_{c2D}, V_{c2Q}	Double fundamental frequency components of SM capacitor voltages
B_c	Susceptance of SM capacitor
X_{c2}	Series capacitive reactance of long AC transmission line
P_i, Q_i & P_2, Q_2	The active power and reactive power contributed by fundamental and double frequency components of MMC

References

- [1] "Reader's guide to subsynchronous resonance", *IEEE Transactions on Power Systems*, Vol. 7, No. 1, pp. 150-157, 1992.
- [2] K. R. Padiyar, *Analysis of Subsynchronous Resonance in Power Systems*, Kluwer Academic Publishers, Boston, 1999.
- [3] N. Flourentzou, V. G. Agelidis and G. D. Demetriades, "VSC-Based HVDC Power Transmission Systems: An Overview", *IEEE Transactions on Power Electronics*, Vol. 24, No. 3, pp. 592-602, 2009.
- [4] N. Prabhu and K. R. Padiyar, "Investigation of Subsynchronous Resonance With VSC-Based HVDC Transmission Systems", *IEEE Transactions on Power Delivery*, Vol. 24, No. 1, pp. 433-440, 2009.
- [5] M. Janaki and Nagesh Prabhu and R. Thirumalaivasan and D.P. Kothari, "Mitigation of SSR by subsynchronous current injection with VSC HVDC", *International Journal of Electrical Power & Energy Systems*, Vol. 57, pp. 287-297, 2014.
- [6] T. Joseph, C. E. Ugalde-Loo, S. Balasubramaniam and J. Liang, "Real-Time Estimation and Damping of SSR in a VSC-HVDC Connected Series-Compensated System", *IEEE Transactions on Power Systems*, Vol. 33, No. 6, pp. 7052-7063, 2018.
- [7] A. Lesnicar and R. Marquardt, "An innovative modular multilevel converter topology suitable for a wide power range", *IEEE Bologna Power Tech Conference Proceedings*, Bologna, Italy, Vol. 3, 2003.
- [8] S. Debnath, J. Qin, B. Bahrani, M. Saeedifard and P. Barbosa, "Operation, Control, and Applications of the Modular Multilevel Converter: A Review", *IEEE Transactions on Power Electronics*, Vol. 30, No. 1, pp. 37-53, 2015.
- [9] M. A. Perez, S. Ceballos, G. Konstantinou, J. Pou and R. P. Aguilera, "Modular Multilevel Converters: Recent Achievements and Challenges", *IEEE Open Journal of the Industrial Electronics Society*, Vol. 2, pp. 224-239, 2021.
- [10] J. Sun and H. Liu, "Sequence Impedance Modeling of Modular Multilevel Converters", *IEEE Journal of Emerging and Selected Topics in Power Electronics*, Vol. 5, No. 4, pp. 1427-1443, 2017.
- [11] H. Saad, Y. Fillion, S. Deschamps, Y. Vernay and S. Denetiere, "On Resonances and Harmonics in HVDC-MMC Station Connected to AC Grid", *IEEE Transactions on Power Delivery*, Vol. 32, No. 3, pp. 1565-1573, 2017.
- [12] J. Lyu, X. Cai, M. M. Amin, and M. Molinas, "Sub - synchronous oscillation mechanism and its suppression in MMC - based HVDC connected wind farms", *IET Generation Transmission & Distribution*, Vol. 12, No. 4, pp. 1021-1029, 2018.
- [13] G. Bergna-Diaz, J. Freytes, X. Guillaud, S. D'Arco and J. A. Suul, "Generalized Voltage-Based State-Space Modeling of Modular Multilevel Converters with Constant Equilibrium in Steady State", *IEEE Journal of Emerging and Selected Topics in Power Electronics*, Vol. 6, No. 2, pp. 707-725, 2018.
- [14] A. Jamshidifar and D. Jovicic, "Small-Signal Dynamic DQ Model of Modular Multilevel Converter for System Studies", *IEEE Transactions on Power Delivery*, Vol. 31, No. 1, pp. 191-199, 2016.
- [15] K. Shivashanker and M. Janki, "An approach on nonlinear integration of MMC to linear model of ROPS in transient analysis", *International Journal of Circuit Theory and Applications*, Vol. 51, No. 10, pp. 4584-4606, 2023.
- [16] C. Du, X. Du and C. Tong, "SSR Stable Wind Speed Range Quantification for DFIG-Based

- Wind Power Conversion System Considering Frequency Coupling”, *IEEE Transactions on Sustainable Energy*, Vol. 14, No. 1, pp. 125-139, 2023.
- [17] D. Sun, X. Xie, Y. Liu, K. Wang and M. Ye, “Investigation of SSTI Between Practical MMC-Based VSC-HVDC and Adjacent Turbogenerators Through Modal Signal Injection Test”, *IEEE Transactions on Power Delivery*, Vol. 32, No. 6, pp. 2432-2441, 2017.
- [18] S. Li, X. Huo, Y. Liu and G. Yu, “Design of Sub-synchronous Oscillation Damping Controller in MMC-MTDC for SSO Suppression”, In: *Proc. of 3rd Asia Energy and Electrical Engineering Symposium (AEEES)*, Chengdu, China, pp. 290-294, 2021.
- [19] Chao, Wujie and Deng, Chaoping and Huang, Junwei and Dai, Liyu and Min, Yangxi and Cheng, Yangfan and Wang, Yuhong and Liao, Jianquan, “A Sub-Synchronous Oscillation Suppression Strategy Based on Active Disturbance Rejection Control for Renewable Energy Integration System via MMC-HVDC”, *Electronics*, Vol. 12, 2023.
- [20] Jiang Y, Li K, Cao Y, Zhao L, Jiang X. “Sub-synchronous oscillation suppression in MMC-HVDC grid-connected systems under wind farm fluctuation scenarios”, *Journal of Computational Methods in Science and Engineering*, Vol. 23, No. 1, pp. 405-421, 2023.
- [21] Yu Y, Cheng X, Zhang C, Ji X. “MMC-HVDC system oscillation suppression control strategy based on state feedback decoupling control”, *International Transactions on Electrical Energy Systems*, Vol. 30, No. 11, 2020.
- [22] Y. Miao, X. Zhang, H. Peng, L. Wang and Q. Guo, “Modeling and Oscillation Mechanism Analysis of Renewable Energy Base Connected into MMC-HVDC”, In: *Proc. of Power System and Green Energy Conference (PSGEC)*, Shanghai, China, pp. 203-209, 2023.
- [23] Janaki Muneappa Reddy and Thirumalaivasan Rajaram and Yunjian Xu, “Modal Analysis on Control Impact of Fully Rated Converters-Based PMSG-WECS Connected to Turbine-Generator”, *Electric Power Components and Systems*, Vol. 49, No. 9-10, pp. 930-942, 2021.
- [24] C. Guo, L. Xu, S. Yang and W. Jiang, “A Supplementary Damping Control for MMC-HVDC System to Mitigate the Low-Frequency Oscillation Under Low Inertia Condition”, *IEEE Transactions on Power Delivery*, Vol. 38, No. 1, pp. 287-298, 2023.
- [25] “First benchmark model for computer simulation of subsynchronous resonance”, *IEEE Transactions on Power Apparatus and Systems*, Vol. 96, No. 5, pp. 1565-1572, 1977.
- [26] Shivashanker, K. and M. Janaki, “Design of Decoupled Current Controller for Grid Connected Modular Multilevel Converter”, *International Journal of Emerging Trends in Engineering Research*, Vol. 8, No. 8, pp. 4508-4514, 2020.
- [27] K. Shivashanker, M. Janaki and R. Thirumalaivasan, “Design of Decoupled Current Controller for Back to Back Modular Multilevel Converter Based HVDC Transmission System”, In: *Proc. of Innovations in Power and Advanced Computing Technologies (i-PACT)*, Kuala Lumpur, Malaysia, pp. 1-5, 2021.
- [28] J. Wang and P. Wang, “Power Decoupling Control for Modular Multilevel Converter”, *IEEE Transactions on Power Electronics*, Vol. 33, No. 11, pp. 9296-9309, 2018.